This article is part of a new thematic series on **Computational Approaches to Cardiac Arrhythmias: Translation Into Diagnostics and Therapy,** which includes the following articles:

Introduction to the Series on Computational Approaches to Cardiac Arrhythmias: Translation Into Diagnostics and Therapy [*Circ Res*. 2013;112:831–833.]

Three-Dimensional Impulse Propagation in Myocardium: Arrhythmogenic Mechanisms at the Tissue Level [*Circ Res*. 2013;112:834–848.]

Rotors and the Dynamics of Cardiac Fibrillation

Noninvasive Electrocardiographic Imaging of Arrhythmogenic Substrates in Humans

Jose Jalife, Guest Editor

Rotors and the Dynamics of Cardiac Fibrillation

Sandeep V. Pandit, José Jalife

Abstract: **The objective of this article is to present a broad review of the role of cardiac electric rotors and their accompanying spiral waves in the mechanism of cardiac fibrillation. At the outset, we present a brief historical overview regarding reentry and then discuss the basic concepts and terminologies pertaining to rotors and their initiation. Thereafter, the intrinsic properties of rotors and spiral waves, including phase singularities, wavefront curvature, and dominant frequency maps, are discussed. The implications of rotor dynamics for the spatiotemporal organization of fibrillation, independent of the species being studied, are described next. The knowledge gained regarding the role of cardiac structure in the initiation or maintenance of rotors and the ionic bases of spiral waves in the past 2 decades, as well as the significance for drug therapy, is reviewed subsequently. We conclude by examining recent evidence suggesting that rotors are critical in sustaining both atrial and ventricular fibrillation in the human heart and its implications for treatment with radiofrequency ablation. (*Circ Res*. 2013;112:849-862.)**

Key Words: atrial fibrillation ■ spiral waves ■ ventricular fibrillation ■ wavebreak ■ wavefront curvature

The term "rotor" is becoming a household name in cardiac electrophysiology. It applies to the organizing source of functional reentrant activity, particularly in the context of tachycardia and fibrillation. Emerging evidence clearly supports a major role for rotors as the drivers of cardiac fibrillation in animal models and in humans. Remarkably, much of what we have learned about the dynamics of rotors and the spiral waves generated by them derives from the field of computational biology and from the study of wave propagation in excitable media. In the heart, the atria and ventricles share similar dynamics of electric wave propagation despite their vastly different geometry, global structure, and ionic mechanisms. More importantly, the behaviors of the electric rotors and spiral waves that form in their respective walls are also similar and may be analyzed using tools derived from the study of nonlinear systems. Thus, we make an attempt to reconcile such concepts with the more traditional ideas about mechanisms of cardiac fibrillation. First we set our current knowledge of reentry in a historical context, and then briefly define the basic notions and the terminology used throughout the article. Subsequently, we review our current understanding of how rotors are initiated and the technologies that are used to localize them in the atria or ventricles, as well as to quantify their properties, including their dynamics and frequency of activation. We then present evidence demonstrating the similarities in the dynamics of rotors and their

Original received September 26, 2012; revision received November 1; 2012, accepted November 12, 2012, In December 2012, the average time from submission to first decision for all original research papers submitted to *Circulation Research* was 14.5 days.

From the Center for Arrhythmia Research, Department of Internal Medicine-Cardiology, University of Michigan, Ann Arbor, MI.

Correspondence to José Jalife, Center for Arrhythmia Research, University of Michigan, NCRC, 2800 Plymouth Rd, Ann Arbor, MI 48109. E-mail jjalife@med.umich.edu

Circulation Research **is available at http://circres.ahajournals.org** **DOI: 10.1161/CIRCRESAHA.111.300158**

Nonstandard Abbreviations and Acronyms

2D	two-dimensional
AF	atrial fibrillation
APD	action potential duration
BM	body mass
DF	dominant frequency
h	fast inactivation variable of the sodium current
I_{k1}	inward rectifier K^+ channel
j	slow inactivation variable of the sodium current
LA	left atrium
NRVM	neonatal rat ventricular myocyte
PS	phase singularity
PV	pulmonary vein
R	radius of wavefront curvature
RA	right atrium
RCr	critical radius of wavefront curvature
TG	transgenic
VF	ventricular fibrillation
VT	ventricular tachycardia

consequences that exist in all mammals, including humans. Here, we give attention to universal scaling laws that may govern such similarities. Thereafter, we focus on triggers and substrate as the essential factors involved, respectively, in the mechanisms of initiation and maintenance of rotors, followed by the ionic bases of rotor dynamics and the manner in which antiarrhythmic drugs can modify rotor behavior. We close the article by briefly looking into new evidence supporting the idea that rotors may be critical in sustaining both atrial fibrillation (AF) and ventricular fibrillation (VF) in the human heart and the manner in which such evidence might lead to more mechanistic approaches to effectively terminate AF in the clinical electrophysiology laboratory.

Evolving Theories About Reentry Over the Past Century

The topic of the history of reentry has been reviewed in detail recently.[1] Only the main points are highlighted here. Studies of fibrillation and its mechanisms have been performed since the turn of the 20th century. The first known experiments were conducted by Mayer[2] in jellyfish rings and turtle ventricular muscle in 1906. In Mayer's experiments,[2] isolated rings of muscle could sustain circulating activity for long periods of time. Soon thereafter, the studies of Mines and Garrey[3–5] in rings of canine ventricular muscle formed the basis for the concept of anatomic reentry as we know it today. Lewis[6–8] postulated that AF and atrial flutter could be attributed to a circulating reentrant wavefront that encroached on its own partially refractory tail. The main difference between fibrillation and flutter was the gap or the nature of the encroachment of the front into the tail: the gap was fully excitable and quite large in flutter, whereas it was smaller and partially excitable in AF, because of the intermingled front and tail. These ideas progressed forward in the 1940s with the theoretical studies of Wiener and Rosenblueth,[9] who postulated that reentry around an obstacle was necessary to sustain fibrillation. In the 1960s, Moe[10] challenged the prevalent concepts about reentry by postulating that instead of a single reentrant circuit, multiple randomly propagating wavelets were responsible for sustaining AF. Remarkably, Moe's hypothesis[10] was partly based on results obtained via innovative computer modeling studies.[11] In the 1970s, Allessie et al[12–14] proposed the leading circle hypothesis based on experiments conducted in the rabbit atrial muscle, in which electrical waves rotated around a functional obstacle. Subsequently, in 1985, Allessie et al[15] provided the first experimental proof for Moe's multiple wavelet hypothesis[10] of AF in the canine atria. Meanwhile, the concept of rotors generating spiral waves was being developed in parallel via theoretical studies conducted in the erstwhile Union of Soviet Socialist Republics by Krinsky[16] and in the United States by Winfree.[17] It was proposed that these reverberators or rotors also could exist in the heart and underlie functional reentry. The first experimental demonstration of a spiral wave in the heart was made in an isolated sheep ventricular muscle slice by Davidenko et al in 1990.[18] This was mainly possible because of the use of voltage-sensitive dyes that allowed for high-resolution mapping of the cardiac electrical activity.[19] The subsequent 2 decades have seen a vast amount of knowledge gained regarding rotors, spiral waves, and their underlying mechanisms, partly because of the development of sophisticated tools and algorithms for their analyses, which have led to our current concepts regarding rotors and their role in cardiac fibrillation.[1,20,21] There is still debate about the precise mechanisms of fibrillation (small number of driving sources or rotors vs multiple wavelets).[1,21–24] Nevertheless, the concept of rotors as underlying drivers of fibrillation has driven the field forward and is poised to prove immensely beneficial as both basic scientists and clinical investigators use these ideas in developing mechanism-based therapies and treatment modalities for AF and VF in the next decade.

What Is a Rotor?

The traditional view of a wave propagating in a fixed ring-like path with an excitable gap separating the wavefront from its tail of refractoriness (Figure 1A)[25] is an accurate representation of anatomical reentry. In this model, the wavelength is defined as the spatial extension of the propagating wave (all of the depolarized cells) and computed as the product of the refractory period and the conduction velocity. Functional reentry, however, was initially described via the leading circle hypothesis (Figure 1B).[14] According to this model, reentry requires no anatomical obstacle and there is no fully excitable gap as the circulating excitation wavefront encroaches on its tail. The tissue inside the leading circle is deemed to receive a centripetal excitation wavefront, which renders it refractory. A rotor is a similar form of functional reentrant activity (Figure 1C) but with a critical difference: the curved wavefront and wavetail meet each other at a singularity (white asterisk, Figure 1C), and the tissue at the center is not refractory.[26] The terms "spiral wave" and "rotor" have been used interchangeably by some; however, in the context of cardiac arrhythmias, rotors are drivers or organizing sources of fibrillation, be it AF or VF, and a spiral wave is more accurately a 2-dimensional (2D) representation of the curved vortices generated by the spinning rotor in its immediate surroundings.[1] The 3-dimensional representation

of a spiral wave is termed a "scroll wave," and its center of rotation is a hollow filament formed by the revolving trajectory of the spiral tip (Figure 1D). The latter represents the core of the spiral viewed from one surface, as depicted with the broken circle in Figure 1E. The presence of both scroll waves and filaments has been demonstrated in the heart in both numerical[27] and experimental studies.[28]

A schematic representation of a rotor generating spiral waves is illustrated in Figure 1E to allow for a closer look at the curved activation wavefront, the curved wavetail, and the point at which wavefront and wavetail meet. The wavefront represents an area of depolarized cells as the cardiac impulse travels forward, and the wavetail comprises the group of cells that have undergone full excitation (action potential upstroke) and are returning to rest (action potential repolarization). As discussed in detail, in 1998, Gray et al[29] developed a technique based on phase plane analysis to investigate cardiac fibrillation in optical mapping experiments and to identify the rotor, which was demonstrated to be a singularity point or phase singularity (PS), represented in Figure 1E by an asterisk. This allowed for the tracking of the spiral and its tip dynamics, in space, over time. When a rotor is stationary, it pivots as a PS around a circular trajectory forming the core of the spiral wave (Figure 1E); however, when the rotor meanders, its trajectory can take various complex shapes, depending on the tissue excitability.[30] As noted, the 3-dimensional representation of a spiral wave is the scroll wave. If the rotor is completely stationary and spans from the epicardium to the endocardium, then the filament of the spiral would be a linear cylinder (I-shape).[28] The filament can also bend, adopting varying nonlinear shapes (L-shape, U-shape, O-shape, etc).[27] If, however, the scroll wave meanders, then the PS would not form a cylinder but would move along a trajectory of which the complexity will depend on the degree of meandering. In this case, the filament would be a line.

Three important points of difference become immediately apparent between the theory of rotors and the so-called leading circle reentry. First, the leading circle idea does not consider the curvature of the rotating wavefront[31] as a factor controlling the velocity of the impulse and the dynamics of the reentrant activity. The theory of rotors envisions that the propagation velocity of a wavefront in the 2D or 3-dimensional myocardium very much depends on its curvature; waves for which the front is concave propagate faster than planar waves, but the velocity of planar waves is faster than convex waves. Rotating waves consist of wavefronts, and the curvature progressively increases toward the center (the core). At the very tip (the PS), the convex curvature reaches a critical value that makes it impossible for the activity to invade the core. This leads to the second difference: the leading circle assumes full refractoriness at the core, produced by the continuing invasion of centripetal waves forming a ring of excitation around a functionally unexcitable obstacle, not unlike the anatomic obstacle of circus movement reentry similar to that described by Mines.[4] Whether functional or anatomic, the obstacle at the center of the leading circle would make it impossible for the reentry circuit to meander or drift. In contrast, rotors can meander because they pivot around unexcited but eminently excitable tissue.[32] As such, the mechanism underlying the rotation does not depend on the refractoriness at the core but on the exceedingly steep wavefront curvature at the PS, which slows conduction to a critical level that renders the wavefront unable to invade the core.[20] Third, unlike the leading circle, there is no fixed wavelength in rotor-generated spiral waves. In fact, the expanse between the wavefront and the wavetail varies, increasing as a function of the distance (as one goes away) from the PS (Figure 1E). This is because electrotonic gradients established between cells at the core and cells in the near vicinity significantly shorten the action potentials of cells near the core.[25] This point is particularly important because concepts regarding wavelength prolongation are frequently used in the literature, such as for quantifying the effects of antiarrhythmic drugs.[33–35] The spiral wave properties remind us that the wavelength is variable and should be used with caution. More accurate quantification of drug effects on reentry would be obtained by studying how the drug changes the spinning frequency of the rotor (discussed later), as well as its degree of meandering and the number of wavebreaks that its spiraling waves undergo in the periphery, as it happens in fibrillatory conduction.[36]

Another important concept in reentry is the so-called excitable gap.[37] Analyzing the rotor and spiral wave properties allows one to discern this variable in a clear and quantifiable fashion, as shown in Figure 1F. This figure shows a snapshot of a simulated rotor generated in a 2D sheet that incorporated numeric ionic models of human atrial cells.[38] Each cell in the sheet mimics the electrical action potential phenotype seen in persistent AF.[39,40] The top panel shows a snapshot of membrane voltage distribution in the sheet. One can appreciate how current from a depolarized group of cells (red/orange, representing the wavefront) invades the resting cells/tissue in front of it (in dark blue). The bottom panel shows a plot of the product of the variables "h.j", which represents the fast (h) and slow inactivation variables (j) of the Na^+ current, I_{Na},[41] which is the main ionic current driving the spiral wavefront. These variables represent the availability of I_{Na}, and their value varies between 0.0 and 1.0. In other words, when "h.j" is 0.0, no I_{Na} is available, and the tissue is unexcitable (the white area in the bottom panel of Figure 1F), whereas a value of 1.0 means that the tissue is fully available for excitation. All of the other values between 1.0 and 0.0 represent the excitable tissue or gap, where I_{Na} is available, and a stimulus in this area may elicit a response. Thus, the excitable gap underlying a spiral in a 2D sheet also takes a spiral shape (Figure 1F).

Initiation of Rotors and Spiral Waves via Vortex Shedding

A rotor may be initiated in multiple ways.[30] This can involve standard cross-field stimulation protocols in theoretical studies,[38,42] where a plane wave generated by a linear stimulus applied at 1 side of a cardiac tissue sheet is followed by a second stimulus applied perpendicularly while the tissue is only partially recovered. The second stimulus, when timed appropriately and when located spatially in the refractory tail of the first wavefront, can lead to wavebreak and initiate a rotor. Similarly, a rotor can be initiated by unidirectional conduction block in cardiac tissue, resulting from tissue heterogeneities in excitability, repolarization, or conduction

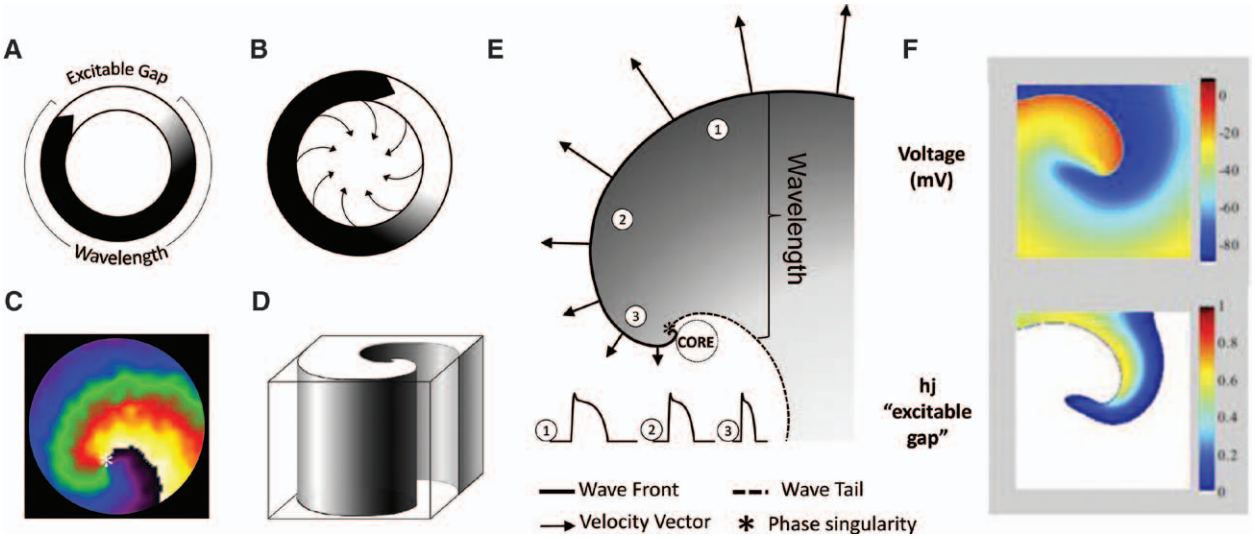

Figure 1. Rotors and spirals, basic concepts. A, Schematic representation of reentry around a ring-like anatomic obstacle where the wavelength (black) is shorter than the path length, allowing for a fully excitable gap (white). **B**, Leading circle reentry around a functional obstacle, with centripetal forces pointing inwards toward a refractory center. **C**, Two-dimensional (2D) spiral wave, along with the rotor tip at the center (*). **D**, Schematic of a 3-dimensional scroll wave. **E**, Snapshot of the spiral wave: electrotonic effects of the core decrease conduction velocity (**arrows**), action potential duration (representative examples shown from positions 1, 2, and 3), and wavelength (the distance from the wavefront [black line] to the wave tail [dashed line]). Conduction velocity (CV) decreases and wavefront curvature becomes more pronounced, near the rotor, which is a phase singularity at the point where the wavefront and the wave tail meet (*). **F**, Computer simulation of reentry.[38] **Top**, Snapshot of the transmembrane voltage distribution during simulated reentry in chronic atrial fibrillation (AF) conditions in a 2D sheet incorporating human atrial ionic math models. **Bottom**, Snapshot of inactivation variables of sodium current, "h.j," during reentry.

velocity[43] or even dynamical properties such as action potential alternans.[44] The underlying basis for rotor and spiral wave initiation is also explained by the phenomenon known as "vortex shedding,"[46] which occurs when a wave encounters an obstacle with sharp edges. Vortex shedding is analogous to the formation of eddies and turbulence, when a water flow reaches a bifurcation or interacts with a narrow barrier, and is rooted in the concept of critical curvature.[45] In brief, as discussed, a planar wavefront propagates faster than a convex wavefront; in fact, the greater the wavefront curvature, the

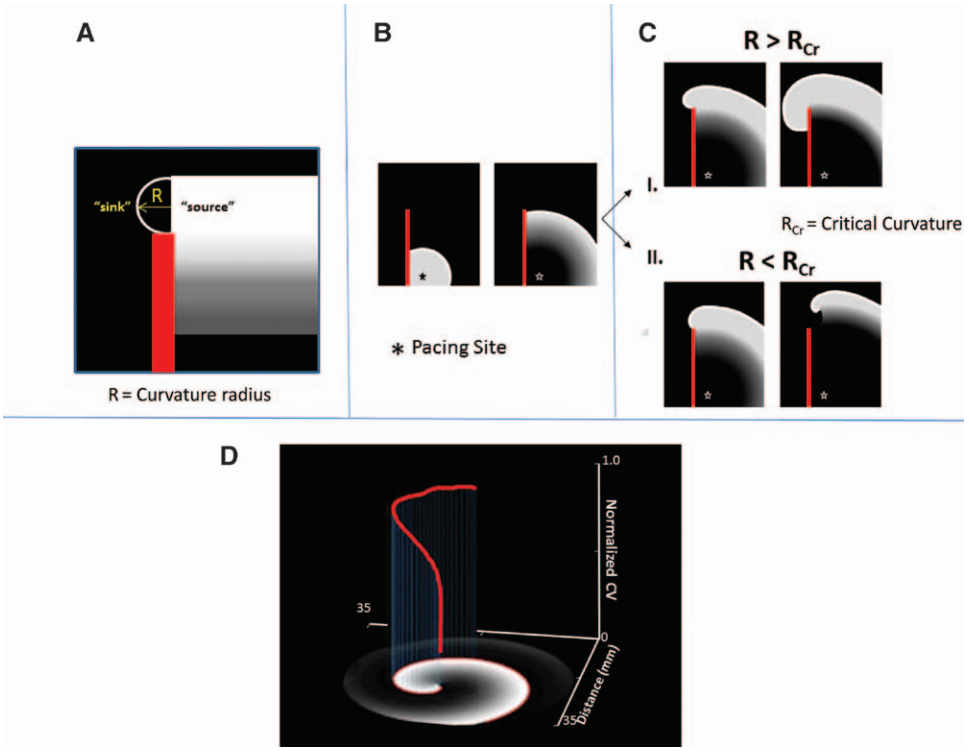

Figure 2. Rotor initiation, vortex shedding. A, Schematic of the mechanism of detachment. Definition of the radius of curvature R of the propagating wavefront (source) as it is about to invade the excitable but nonexcited tissue (sink). **B**, As a wave progresses along an obstacle (red line), the curvature of the wave at the edge of the obstacle will determine whether the wave detaches. **C**, If the curvature of the wavefront (R) at the edge of the obstacle is greater than the critical curvature for detachment (RCr), then the wave remains attached; if R is less than RCr, then the wave will detach from the obstacle and initiate reentry. **D**, Three-dimensional plot illustrating the effect that the wavefront curvature at progressively shorter distances (*x* and *y* axes) from the core has on normalized conduction velocity (red, *z* axis) in a Luo and Rudy[47] computer simulation of reentry.

slower the conduction velocity, up to a critical level at which propagation cannot occur.

The mechanism of vortex shedding was explained by Cabo et al[46] on the basis of the concept of wavefront curvature (R). Figure 2A shows a schematic representation of R, at a time when the wavefront (white) reaches the edge of the obstacle (red). The white curve bounds the area adjacent to the obstacle, which needs to propagate to the left to circumnavigate the obstacle. The radius R of this area is comparable to the width of the wavefront, which determines whether that wavefront (ie, the source) will be able to excite the tissue ahead of it (ie, the sink). In a series of experiments and concomitant simulations, Cabo et al[46] demonstrated the principle of wavebreak generated by vortex shedding. In simulations, they used a 2D sheet of ventricular cells incorporating the 1991 kinetics of Luo and Rudy.[47] For experiments, they used a thin slice of sheep ventricular epicardium; the slice was perfused with a voltage-sensitive dye and optically mapped.[46] An artificial linear obstacle was etched into the ventricular muscle sheet in both simulations and experiments (depicted in a cartoon in Figure 2B, where the obstacle is represented by a red line). As illustrated by the top panel of Figure 2C (condition I), when the excitability of the tissue was normal and a wave was initiated by a point stimulus near the lower right margin of the obstacle (asterisk), the wavefront proceeded to circumnavigate the obstacle without breaking or detaching from it, eventually extinguishing after activating the entire sheet.[46] As shown by the lower panel of Figure 2C, when the excitability of the tissue was diminished somewhat (condition II), either by reducing the maximum conductance of I_{Na} by 75% in simulations or by superfusing the tissue with the sodium channel blocker tetrodotoxin (TTX) in experiments, the same stimulation protocol yielded completely different results: now the wavefront moved upward but detached from the obstacle, curled, and began to rotate around its broken tip, generating a vortex.[46] In the top panel of Figure 2C (condition I), R is larger than the minimum radius of excitation or critical curvature R_{Cr}. Under these conditions, the front progresses laterally without detachment, successfully circumnavigating the obstacle. When $R < R_{Cr}$, (condition II) then the wavefront curls, eventually detaching from the obstacle to generate a vortex around a PS. From the study of Cabo et al,[46] one can infer how pathophysiological conditions such as ischemia or an infarct in the ventricles or atrial remodeling because of persistent AF, in which both I_{Na} density and excitability are reduced and numerous obstacles in the form of patchy fibrotic tissue exist,[48–50] setting the stage for initiation of the rotors that maintain tachycardia or fibrillation.

The inability of the excitation wavefront to depolarize tissue at the PS and its tendency to curve underlies rotor initiation and is important in rotor maintenance as well.[46] The latter is demonstrated in Figure 2D, in which the normalized conduction velocity of the spiral excitation wavefront is plotted vs the distance from its tip (red line in the *z* axis).[1] It can be seen that the wavefront curvature is highest at the tip, and this results in a lesser conduction velocity near the rotation center. Away from the tip, the curvature is reduced and the normalized conduction velocity increases.[1] At the tip, there is constant mismatch between the amount of current needed to depolarize tissue ahead of the wavefront (sink) and the amount of depolarizing current available at the wavefront (source) in play, which causes the rotor to pivot or to meander in complex trajectories. If enough excitable tissue is available, then sustained reentry will occur. Thus, wavefront curvature–related sink-to-source mismatch at the tip is responsible for both rotor initiation (vortex shedding) and maintenance.

Phase Mapping of Rotors and Singularities

A step forward in the analysis of rotor dynamics was the development of the phase mapping technique by Gray et al in 1998.[29] Figure 3A shows a typical optical signal recorded from a point on the epicardial surface of a rabbit heart during VF. We call this time series F(t), where "t" is time. In Figure 3B, the same signal was plotted in 2D phase space as $F(t+\tau)$ vs F(t), where τ is an embedded delay. This approach revealed trajectories rotating around a circle in the center. Then a phase variable "θ" was computed at each site on the cardiac surface and was defined as $\theta(t) = \arctan[F(t+\tau) - F_{mean}, F(t) - F_{mean}]$, where F_{mean} = threshold value, defined as mean value of 4 seconds of VF activity and $\tau \approx$ ¼ the value of the cycle length during fibrillation.

Phase mapping allowed for the generation of color phase movies and the quantification of rotor dynamics, which led to the clear identification of PS points, as illustrated in Figure 3C. Each color represents a phase in the excitation recovery cycle, and a PS is defined as a site where all of the phases converge, because at the PS the phase is arbitrary; in contrast, the surrounding elements exhibit a continuous progression of phase that is equal to $\pm 2\pi$ around the PS.[29] The original approach of plotting the dynamics on phase space has allowed investigators to systematically study the initiation, maintenance, and termination of rotors in normal and pathophysiological conditions.[51] However, the approach requires a careful choice of the embedded delay τ. More recently, a Hilbert transform–based approach facilitated computing the instantaneous phase.[52,53] Regardless of the approach, it is clear that wavebreak and formation of a PS are essential conditions for a rotor to exist. Moreover, we have learned through experiments and simulations that rotors need not be stationary but may meander over complex trajectories,[54] giving rise to irregular electrograms (Figure 3D).[55] In many cases, fibrillation is terminated because of a PS colliding with a boundary,[42,51] thereby extinguishing the spiral waves.

Dominant Frequency Mapping

In the late 1990s and early 2000s, experimental mapping of both AF and VF in isolated hearts of various animal models using optical imaging demonstrated that rotors, whether single, in small numbers, or sometimes multiple, were consistently detected during cardiac reentry.[56,57] It was possible to visualize the rotors and phase mapping also allowed tracking of their spatiotemporal dynamics, revealing that rotors were either stable, as in monomorphic ventricular tachycardia (VT), or constantly meandered over complex trajectories, as in polymorphic VT.[51] The meandering rotors also were postulated to underlie both torsade de pointes,[58] as well as VF.[59] A further important development in the analysis of rotors occurred when their time-dependent behavior was analyzed in the frequency domain.[60] Fast Fourier transform analysis of

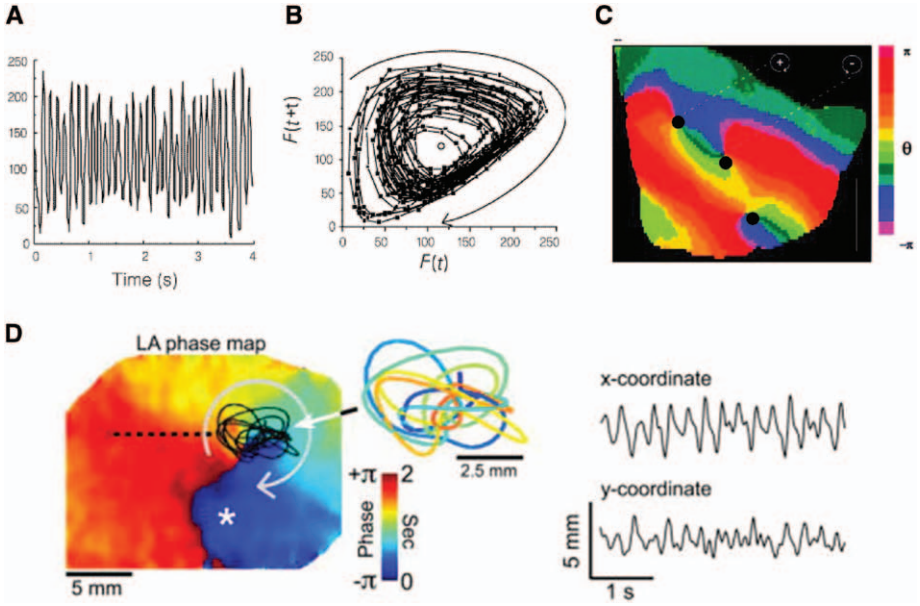

Figure 3. . Singularity points revealed by phase plane analysis.[29] A, Optical signal in time domain at a given point on the surface of a rabbit ventricle during ventricular fibrillation (VF).[29] **B**, Phase plane analysis, where optical signal with embedded delay F(t+τ) is plotted against itself F(t).[29] **C**, Phase movie during VF, with identification of rotors or phase singularities (PS), as dark black dots, at points where all phases (colors) converge. **D**, Rotor meandering and fractionation in optical mapping experiment during atrial fibrillation (AF) in isolated sheep heart. On the **left**, a left atrial phase snapshot demonstrates reentrant activity in the left atrium (LA) free wall. The **inset** shows the time–space trajectory of the tip; the x and y coordinate signals are shown on the **right**. Modified from Zlochiver et al.[55]

optical signals within a given time window across vast extensions of the epicardial surface of the fibrillating atria or ventricles yielded a spatial frequency map of the signals in the area of interest.[57,60,61] Selecting the maximum frequency in the Fourier spectrum of each recording location allowed for the construction of so-called dominant frequency (DF) maps, as shown in Figure 4.[61] Examples of optical and electrical signals from the left atrium (LA) and the right atrium (RA) of

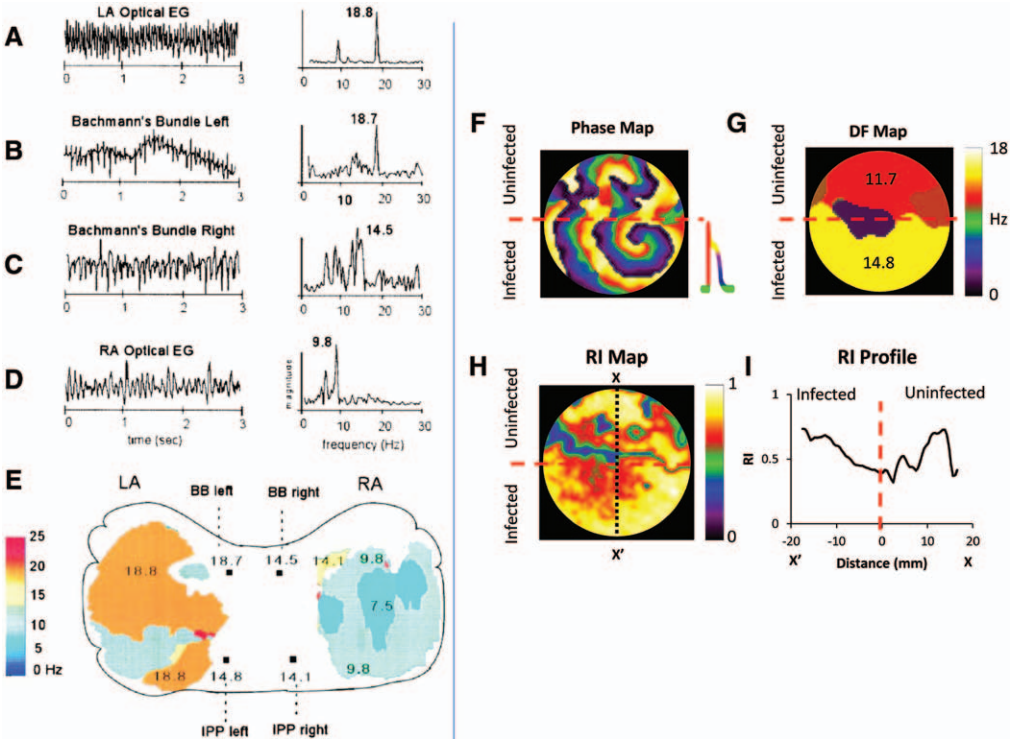

Figure 4. Dominant frequency (DF) analysis of rotors and fibrillatory conduction. A–D, Time-dependent optical signals and electrograms (**left**) and corresponding fast Fourier transform (FFT; **right**) from the left atrium (LA), Bachmann bundle (**left**), Bachmann bundle (**right**), and right atrium (RA) during atrial fibrillation (AF) induced in the presence of acetylcholine in an isolated, Langendorff-perfused sheep heart. **E**, DF map of areas within the LA and RA showing a left-to-right DF gradient during AF. **A–E**, From Jalife and Gray.[59] **F**, Phase map of a regionally adenovirus-hERG–infected neonatal rat ventricular myocyte monolayer showing a fast stable rotor within the infected region (below red dashed line) and patterns of wavebreak and fibrillatory conduction in the uninfected region (above red dashed line).[70] **G**, DF map demonstrating a frequency gradient between uninfected and hERG-overexpressing regions, with an increased frequency of activation within the infected region. **H**, Regularity index (RI) map showing a decrease (blue) in the regularity of activation at the hERG and action potential duration (APD) gradient region. **I**, RI profile (taken at the black dotted line, along X-X′) further illustrating that the region of greatest wave disruption occurs at the hERG/APD gradient (red dashed line).

sheep and their respective power spectra obtained during AF induced via burst pacing in the presence of acetylcholine are shown (Figure 4A–4D). The 3-second time-dependent signals are on the left, and their corresponding frequency spectra obtained after fast Fourier transform analysis are on the right. Although multiple peaks of frequency can be observed in the individual spectra, dominant peaks of frequency can be identified in all. In Figure 4E, DF peaks from multiple locations recorded with a charge-coupled device camera in a 5-second optical mapping movie are plotted as DF maps superimposed on a schematic representation of the sheep LA and RA.[61] A consistent finding in power spectral analyses obtained in this manner was that, in a majority of the experiments, the frequency of atrial activation during AF was higher in the LA compared with the RA. This finding has been replicated for AF in other species, such as pigs,[62] and also in the electrogram analysis of AF frequencies for paroxysmal AF in humans.[63–65]

Thus, representation of fibrillation in the frequency domain demonstrates that AF[61] (and also VF[66]), rather than being the result of randomly propagating wavelets, shows a consistent spatial organization of frequencies, which is chamber-dependent. This has led to the following postulates. First, a spatially distributed hierarchy of DFs of excitation indicates that, in most cases, AF is sustained by a small number of high-frequency drivers (rotors) in the LA that maintain the overall activity. Second, the DF of the rotor(s) is exceedingly high and, therefore, can only drive in a 1:1 fashion the tissue in its immediate surroundings. Beyond this 1:1 domain, the wavefronts undergo intermittent, spatially distributed wavebreaks, with the end result being fibrillatory conduction toward distal areas in both the LA and the RA.[1,61,67] Thus, DF analysis of experimental data provided evidence for organization in some forms of fibrillation,[68] and this experimental observation was also supported by computer simulations,[69] as well as by mapping of rotors in 2D monolayers of rat neonatal ventricular cells, as shown in Figure 4F through 4I.[70] In this representative experiment, the bottom half of the monolayer was infected with an adenoviral construct for the gene coding hERG, the molecular correlate of the rapid delayed rectifier K^+ current, I_{Kr}, whereas the top half was uninfected. This resulted in an I_{Kr} density gradient with higher I_{Kr} current magnitude in the bottom half and sustained rotor formation (Figure 4F).[70] The spiral wavefronts generated by the rotor in the I_{Kr}-infected region blocked intermittently at the interface and could not drive the uninfected region in a 1:1 fashion. Instead, as shown by the DF map in Figure 4G, a frequency gradient was established, with a higher DF in the infected region compared with the uninfected region. These results are similar to the LA-RA gradients in cholinergic AF experiments in sheep (Figure 4E)[60,61] and paroxysmal AF in humans.[63–65] In addition, when a regularity index, defined as the ratio of DF:total spectral power, was calculated for each video camera pixel recording the potentiometric dye fluorescence changes in the 2D monolayer, the values were unequally distributed. A vertical line (X-X′) drawn in the 2D monolayer dish (Figure 4H) showed the regularity index to be lowest at the interface between the infected and the uninfected regions (Figure 4I).[70] These data suggest that the most complex fractionation of the signal is observed at the interface/boundary between the hERG-infected and noninfected regions, where there is a sharp change in refractoriness (because of changes in density of I_{Kr}). Altogether, DF mapping has allowed for the demonstration that fibrillation is deterministic and displays organization, with a hierarchy of frequencies indicating underlying chamber-specific ion channel gradients, and the location of complex fractionated signals, which are at the periphery of the rotors.

Universal Scaling of Fibrillation Frequency

Mechanisms of fibrillation are being investigated in many laboratories using hearts from a variety of species, ranging from the mouse to much larger mammals, including dogs, sheep, goats, and pigs, as well as explanted human hearts. Thus, important questions arise regarding whether rotors can be observed across different species and whether the rotor properties obey common laws. The questions are motivated in part by the long-held contention that fibrillation cannot sustain in cardiac tissue for which mass is lower than critical.[71] This critical mass idea was first challenged by the studies of Vaidya et al,[72] who showed that with burst pacing, one could create conditions in small mouse hearts for functional reentry and sustained VF, and that rotors could be observed in an area as small as 100 mm^2. By the mid 2000s, rotors and spiral waves had been demonstrated in isolated hearts from mice, rats, guinea pigs, rabbits, sheep, pigs, and dogs. To understand their common link, Noujaim et al[73] endeavored to quantify the relationship between body mass (BM) and VF frequencies. They were partly motivated by previous studies in which it was shown that many biological phenomena, such as metabolic rate, life span, respiratory rate, and ECG parameters like the PR interval scale with BM.[74] The general relationship is $Y = a \times (BM)^b$, where Y is the biological variable of interest, "a" is a constant, and "b" represents the scaling exponent.[73] Results obtained by Noujaim et al[73] are reproduced in Figure 5. Figure 5A shows DF maps obtained in optical experiments during VF in a mouse, a guinea pig, a rabbit, and a human heart with body weights of 30 g, 600 g, 3 kg, and 90 kg, respectively. In each map, the DF domain is indicated in red as follows: 38.0 Hz for the mouse; 26.0 Hz for the guinea pig; 15.0 Hz for the rabbit; and 6.8 Hz for the human heart. Notice that although the body weight changes 4 orders of magnitude from mouse to human, the DF changes only 1 order of magnitude. In Figure 5B, a meta-analysis of data collected from 40 studies in 11 different species, from mouse to horse, is plotted as VF frequency vs BM on a double-logarithmic graph.[73] Fitting the data points revealed that VF frequency is $\approx 18.9 \times BM^{-1/4}$; in other words, VF cycle length turned out to be $\approx 53.0 \times BM^{1/4}$. Thus, analysis of VF in the frequency domain allowed for an all-inclusive pattern to emerge across mammalian species. The underlying mechanisms have not been elucidated completely, but it seems clear that changes in the species-related action potential duration (APD), along with the heart size, play a significant role.[73]

Triggers, Cardiac Structure, and the Formation and Maintenance of Rotors

The onset and maintenance of cardiac fibrillation require an event (trigger) that initiates the arrhythmia and the presence of a predisposing substrate that perpetuates it. In AF, well-known clinical studies have demonstrated that the majority of

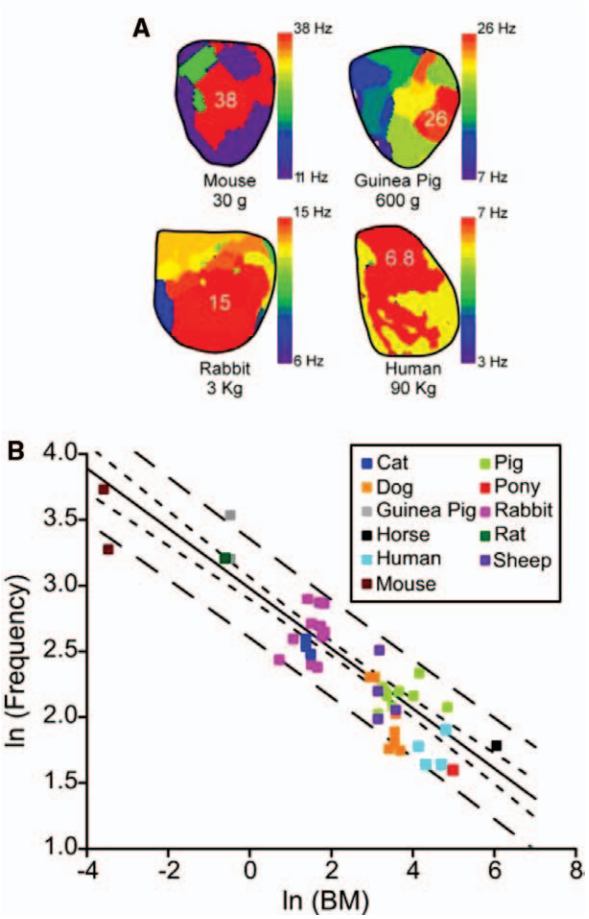

Figure 5. Scaling of frequency of rotors and fibrillation.[73] **A**, Dominant frequency (DF) maps during ventricular fibrillation (VF) in mouse, guinea pig, rabbit, and humans. **B**, Double-logarithmic plot of DF vs body mass in different species.

ectopic discharges initiating the arrhythmia emerge from the pulmonary vein (PV) sleeves,[75] which are known to terminate in dead-end pathways. In some patients, the electric properties of the muscle bundles in the PV sleeves seem to make them highly prone to generate high-frequency automatic or triggered discharges, which propagate into the posterior LA wall, of which the highly heterogeneous and anisotropic fiber bundle arrangements and abrupt changes in thickness[76] provide an ideal substrate for sink-to-source mismatch, wavebreak, and reentry formation. In a recent study in which brief trains of electric stimuli were used to trigger PV discharges at a high frequency, most of the wavebreaks that initiated AF appeared at the septal side of the septopulmonary bundle near the right superior PV, where the myocardial thickness dramatically expands.[77] It was clear that the source current provided by certain PV impulses was insufficient to overcome the vast sink of the transition posterior LA septum, which resulted in wavebreak, reentry, and AF. A somewhat different but related mechanism can initiate reentry and fibrillation in the ventricles. For example, at the Purkinje–muscle junction,[78] anatomic expansions are prone to conduction delays and block specifically in areas of abrupt electric current source-to-sink mismatch.[79] As discussed for the study of Cabo et al,[46] whether in the atria or ventricles, source-to-sink unbalance can explain wave detachment from obstacles and vortex shedding leading to rotors and fibrillation.

Once initiated, rotors will spin at very high rates to generate electric turbulence (fibrillatory conduction). Recently, using a chronic RA tachypacing model of persistent AF in the sheep, along with continuous cardiac rhythm monitoring by dual implantable devices, we demonstrated that rotors are capable of maintaining cardiac fibrillation in the long-term, even after both structural and electric remodeling have taken place.[80] We demonstrated that in vivo DF values during AF progressively

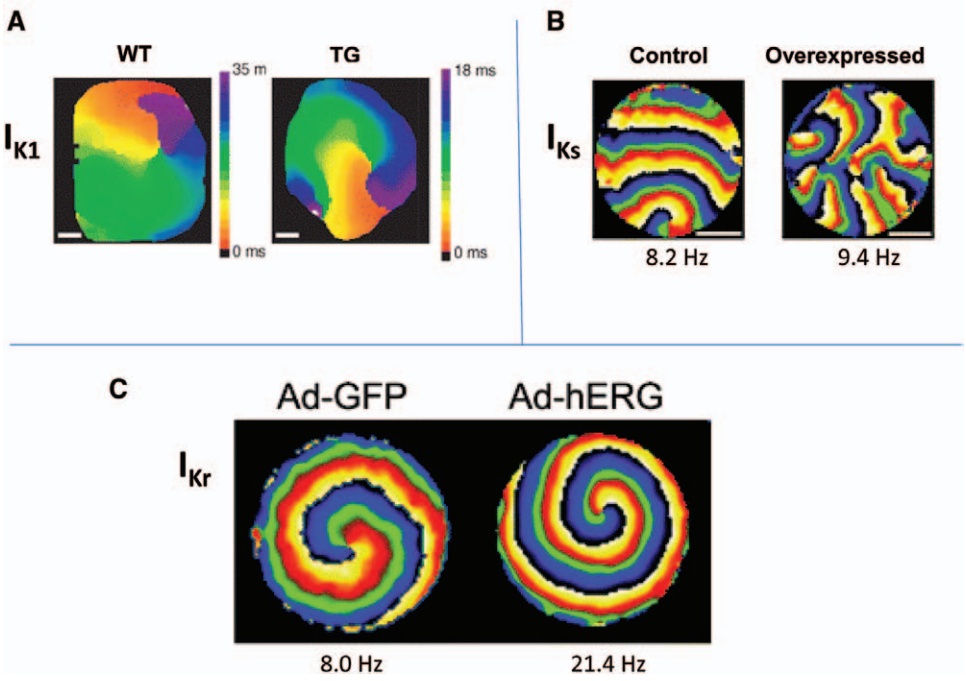

Figure 6. Rotors, ionic basis. A, Rotors in wild-type (WT) and transgenic (TG) mouse hearts where inward rectifier K^+ channel (I_{K1}) was overexpressed.[105] **B**, Rotors in a control neonatal rat ventricular myocyte (NRVM) monolayer and a similar monolayer in which I_{Ks} was overexpressed via adenovirus.[107] **C**, Rotors in a control NRVM monolayer and a similar monolayer where I_{Kr} was overexpressed via adenovirus.[108]

increased while preserving in the long-term a DF difference between the LA and the RA. After follow-up periods of 9 to 24 weeks, mapping of the atria and subsequent structural analyses ex vivo confirmed the presence of DF gradients from posterior LA to RA, together with patterns of activation, all of which were consistent with the contention that rotors in an enlarged LA are fully capable of maintaining AF dynamics in the long-term. Similar to AF, the papillary muscle ventricular structures have been postulated to play an important role in the generation and maintenance of both VF and VT.[81]

The importance of structure in initiating reentry and arrhythmias was further reiterated in recent experiments in monolayers of neonatal rat ventricular myocyte (NRVM) cultures. Auerbach et al[82] showed that in patterned monolayers consisting of 2 wide regions connected by a thin isthmus, reflection and arrhythmogenesis were enhanced. Bian and Tung[83] showed that reentry is readily induced by rapid pacing in NRVM monolayers containing a central and asymmetrical island containing a predefined zigzag pattern.

Ionic Basis of Rotors

Many investigators using either pharmacological tools in experimental animal models or numeric simulations have contributed to our current understanding of the underlying ionic basis for the initiation and maintenance of rotors (only a few are cited here because of space limitations).[84–94] However, the availability of genetic mouse models[95] and the reproducibility of consistent rotors in 2D monolayers of neonatal rat cells,[96,97] coupled with the development of biophysically detailed ionic mathematical models of murine ventricular electrophysiology,[98,99] allowed for a more robust dissection of the contribution of individual ion channels to high-frequency rotors from the year 2000 onward. In this section, we mainly discuss studies performed in our laboratory over the past decade, although we acknowledge the important contributions of numerous other investigators to this particular field.[87–94]

The earliest studies focused on the role of the inward rectifier K^+ channel (I_{K1}). Computer modeling studies of 2D reentry[100] and experimental studies in guinea pig hearts[66] suggested an important role for I_{K1} in the spatiotemporal organization of VF frequencies across different chambers of the heart. The importance of I_{K1} received further support from studies that showed that VF frequencies were slowed and VF was subsequently terminated by $BaCl_2$ at concentrations of 1 to 50 μmol/L, which were relatively selective for I_{K1} blockade.[84] The chamber-specific LA-RA spatiotemporal gradient of AF frequencies in the presence of acetylcholine was attributable to different densities of another inward rectifier K^+ channel, the acetylcholine-activated K^+ current, I_{KACh}.[67] The density of I_{K1} also was found to be upregulated in atrial myocytes isolated from chronic AF patients.[101–103] When computer simulations were conducted to examine the consequences of I_{K1} increase, the rotors were found to be faster, and the tip meander was reduced, being confined to a smaller area, thus stabilizing fibrillation.[38] Those simulations suggested that in addition to causing a shorter APD, I_{K1} accelerated rotors by increasing the availability of I_{Na}; this was possible because of the hyperpolarization of the resting membrane potential by I_{K1}. Although this hyperpolarization was small (≈5 mV), the change in resting membrane potential occurred over the steep portion of the availability curve for I_{Na} and, thus, resulted in a dramatic acceleration of the rotor.

The first direct demonstration of the role of I_{K1} was made possible when transgenic (TG) mice in which I_{K1} was overexpressed became available.[104] Sustained rotors induced in isolated TG mouse hearts were very long-lasting (>1 hour) and extremely fast (≈50–60 Hz); by contrast, in wild-type hearts, rotors were much slower (≈20–25 Hz) and lasted less than ≈10 seconds.[105] In Figure 6A, we compare the activation map of a rotor observed experimentally in a TG mouse with I_{K1} overexpression (right) vs a wild-type heart (left). It is clear that the rotor completes 1 rotation much earlier in the TG mouse (note the different time scales). These experimental results were confirmed in computer simulations, using a detailed ionic mathematical model of the mouse ventricular action potential, which incorporated all of the major K^+ currents recorded experimentally.[105] The simulations further supported a key role for I_{K1} and I_{Na} as important ionic mechanisms determining fast rotor activity.

Although relevant, the studies in the mouse did not reveal the role of the 2 main repolarizing K^+ currents in the human ventricle, that is, the fast and the slow delayed rectifier K^+ currents, namely, I_{Kr} and I_{Ks}.[106] These currents do not contribute in a meaningful way to the short APD in the mouse ventricle.[106] Studies in higher mammalian hearts did show that E-4031, a relatively selective blocker of I_{Kr}, could slow VF frequencies.[94] In addition, in a rabbit model of 2D reentry created via cryoablation of the ventricular endocardium, it was shown that perfusion of nifekalant, a relatively selective blocker of I_{Kr}, terminated rotors mostly because of their collision with the atrioventricular groove.[93] Therefore, we investigated the role of these delayed rectifier K^+ currents in monolayers of confluent electrically coupled NRVM using an approach modified from that described originally by Rohr et al.[96] At 5 to 6 days of age, the action potential of NRVMs present a plateau and APD of ≈200 ms, which would allow both I_{Kr} and I_{Ks} to activate. To further increase the density of either I_{Ks} or I_{Kr}, we used adenoviral transfer of genomic sequences of either KvLQT1-minK or hERG, respectively, in NRVM monolayers and studied their effects on rotor dynamics.[107,108] To our surprise, I_{Ks} overexpression did not increase rotor frequency at all; however, over time, the excessive I_{Ks} caused an increasing number of wavebreaks to occur. This is illustrated in Figure 6B by the representative phase maps in a control monolayer and a monolayer in which I_{Ks} was overexpressed.[107] Experiments in HEK cells and computer simulations suggested that the increased wavebreak incidence observed in monolayers was attributed to the phenomenon of postrepolarization refractoriness because of residual outward I_{Ks} current after the action potential.[107] This phenomenon was demonstrated previously in guinea pig ventricular myocytes in the late 1980s.[109,110]

In Figure 6C, overexpression of I_{Kr} caused the rotor to accelerate significantly compared with control.[107] Concomitant simulations showed that the acceleration attributed to I_{Kr} increase was not comparable with that caused by I_{K1} overexpression.[108] Interestingly, both simulations and experiments showed a novel mechanism underlying rotor acceleration, in addition to APD shortening: transient resting membrane potential

hyperpolarization, which again would indirectly affect rotor frequency by modifying I_{Na} availability.[108] Sekar et al[111] conducted similar experiments with overexpression of I_{K1} in rat neonatal monolayers, which supported the conclusions from our mouse studies.[105]

In addition to K^+ channels, the Ca^{2+} channels and the excitation-contraction (E-C) coupling machinery also influence the cardiac action potential and repolarization,[112] and both are also likely to influence the spiral wave dynamics, although the results remain controversial. In a study from our laboratory that examined the effect of verapamil on VF, the DF was reduced, core meander was increased, and VF was converted to VT.[85] However, these results must be interpreted with caution because at the concentrations of verapamil used in this study, verapamil blocks the L-type Ca^{2+} channel, I_{CaL}, and I_{Kr}.[113] The role of intracellular Ca^{2+} in sustaining VF/spirals is also less clear and remains controversial. Studies from the Zaitsev laboratory[114,115] suggested that intracellular Ca^{2+} action potential dissociation during VF was a consequence, not a cause, of wavebreaks in VF and that no spontaneous voltage-independent intracellular Ca^{2+} waves could be seen. However, others have challenged these findings.[116] In contrast, intracellular Ca^{2+} has been shown to be important in the initiation of spontaneous activity in Torsade de Pointes (TdP)[117] and inherited arrhythmias, such as catecholaminergic polymorphic ventricular tachycardia, which can then give rise to the initiation of rotors and fibrillation.[118] Finally, the Na^+ current, I_{Na}, is key in determining excitability and the upstroke of the cardiac action potentials and is the main current driving the wavefront during normal propagation, as well as during rotor activity. We have assessed the role of I_{Na} in rotor dynamics either directly via TTX, which blocks I_{Na},[86,119] or indirectly by elevating concentrations of extracellular K^+ [42,62] or simulating conditions of global ischemia,[119] which limit the availability of I_{Na} because of a depolarized resting membrane potential. In every case, a reduced I_{Na} decreased the DF of the rotor and increased its meander. If I_{Na} was blocked sufficiently (by TTX or extracellular K^+), then the rotor was terminated by collision with a boundary, abolishing AF or VF. However, in many instances, antiarrhythmic class I drugs that block I_{Na}, such as quinidine, do not always terminate fibrillation but either sustain it[58] or convert it to VT (unpublished observations). TG mice with ablation of *SCN5A*, the gene coding $Na_V1.5$, which is the molecular correlate of I_{Na}, display an increased susceptibility to arrhythmogenesis, including VT/VF.[120]

Antiarrhythmic Drugs and Rotors

A direct consequence of the increase in the knowledge of the ionic mechanisms of rotors has been to understand how this information can be applied to design and select more efficacious antiarrhythmic drugs to treat cardiac fibrillation. As discussed, I_{K1} and I_{Na} seem to have dominant effects on reentry properties (frequency and meander). Thus, we have begun to investigate drugs that can block these channels, particularly I_{K1}, and to examine their putative effects on reentrant activity. We compared the effects of chloroquine, an antimalarial drug, with that of quinidine, a class I antiarrhythmic, on VF and rotor dynamics.[121] Figure 7A shows DF maps during VF in a TG mouse heart overexpressing I_{K1}; the top panel shows the effect of quinidine, whereas the bottom panel depicts the effect of chloroquine, and the former reduced VF frequency but did not terminate the arrhythmia, whereas the latter restored sinus rhythm.[121] The normalized DFs in the absence and presence of quinidine/chloroquine are shown in an aggregate of experiments and demonstrate that chloroquine terminated VF in all of the experiments (Figure 7B). Based on patch-clamp and molecular structure data, we hypothesize that the greater success for terminating VF in the case of chloroquine was, in part, attributed to its greater ability to block I_{K1}. Similar results were observed in a recent study conducted in a sheep model of stretch-induced AF.[122] Figure 7C shows DF maps of the posterior LA during stretch-induced AF in an isolated heart before and after coronary perfusion of chloroquine; the drug reduced the rotor frequency.[122] These data were compared with those of flecainide, another class I antiarrhythmic, as summarized in Figure 7D. Flecainide failed to terminate AF in any experiment but converted while converting AF to atrial tachycardia in 2 of 5 experiments at clinically relevant concentrations.[122] In contrast, chloroquine terminated AF and restored sinus rhythm in 7 of 7 experiments.[122] These initial experiments testify to the applicability of concepts learned through the theory of rotors as a mechanism of both AF and VF, that is, drugs that block I_{K1} likely will have greater potency in abolishing cardiac fibrillation. These studies represent only a beginning and would be strengthened by the design of new drugs that can putatively block I_{Na}/I_{K1} without being proarrhythmic and are tested in different arrhythmia/pathophysiological models. An interesting corollary is the antiarrhythmic effect of regional cooling on the myocardium, which seems to reduce the frequency and then terminates VF by unpinning of rotors, which then drift toward the periphery, away from the cooled region, and extinguish by subsequent collision with a boundary.[123]

Spirals in the Human Heart

Most studies of rotors and their analysis until today have been confined to experimental animal models and numeric simulations. Computer modeling studies conducted in either simplified 2D sheets or complex and geometrically realistic 3-dimensional models of the human atria and ventricles have demonstrated that it is possible to induce sustained rotors that drive both AF[38,124] and VF.[125,126] However, experimental data from humans have been elusive and difficult to obtain. Recent in vivo or epicardial surface mapping studies in humans have demonstrated the presence of rotors during VF.[53,126] Nanthakumar et al[73,127] have demonstrated the presence of rotors or even scroll waves[128] during early VF with electric/optical mapping in Langendorff-perfused human hearts. An optically mapped rotor on the human ventricular epicardial surface is shown[73] (Figure 8A). Another case in point is the recent work of Narayan et al,[129] who have used basket catheters to demonstrate sustained sources, a majority of them consisting of rotors, as key driving mechanisms underlying persistent AF. This study showed that patients with persistent AF had a higher number of sources and also had a shorter cycle length compared with patients in paroxysmal AF.[129] An example of a rotor in the LA generating fibrillatory conduction in the RA during AF is shown in Figure 8B.[129] Even more remarkably, the authors could target

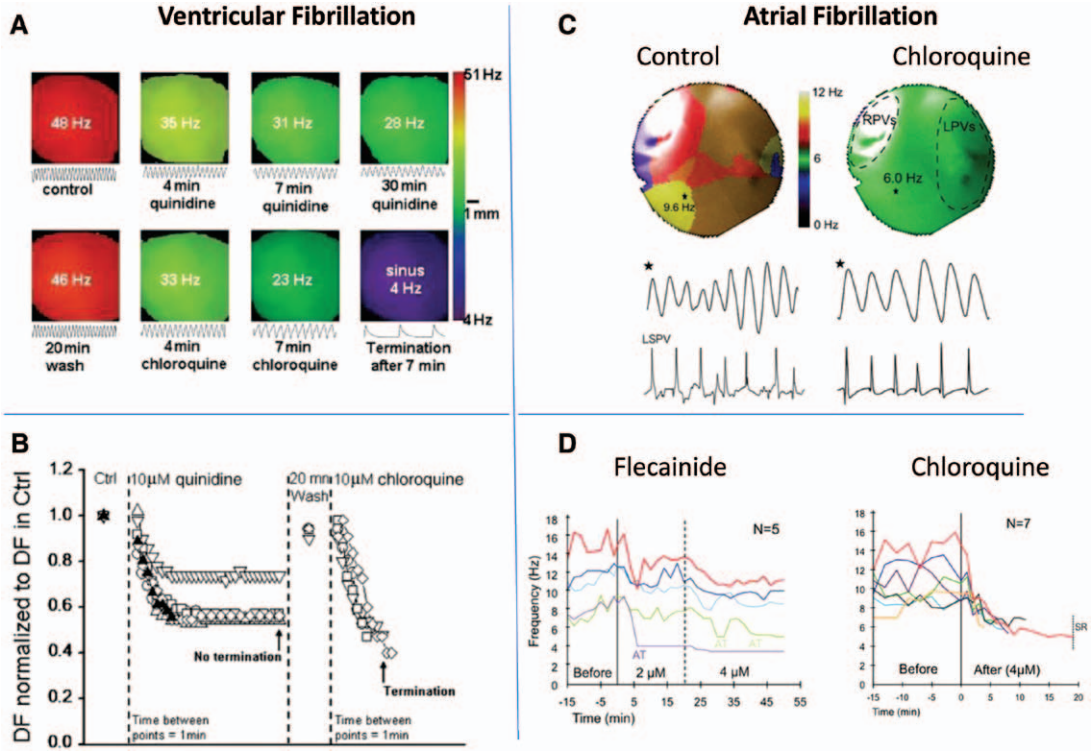

Figure 7. Rotors and antiarrhythmic drugs in ventricular fibrillation (VF) and atrial fibrillation (AF). A, Dominant frequency (DF) maps of VF in inward rectifier K^+ channel (I_{K1})-overexpressing transgenic (TG) mice in the absence and presence of chloroquine.[121] **B**, Comparison of quinidine vs chloroquine effects on normalized DF in VF.[121] **C**, DF maps and underlying optical/electric signals during stretch-induced AF in isolated sheep hearts, in control, and in the presence of chloroquine.[122] **D**, Comparison of the effects of flecainide and chloroquine on the DF during stretch-induced AF in sheep hearts.[122]

these spirals via catheter-based radiofrequency ablation and slow or terminate AF in a manner of minutes rather than hours, as is typically the case.[130] These initial reports are intriguing and exciting. They provide the first support for the role of rotors as key drivers of sustained AF in humans. If reproduced consistently by other laboratories, this mechanistically based approach could substantially improve the safety and the outcome of radiofrequency ablation and benefit many patients.

Conclusions

Emerging evidence clearly supports a major role for rotors as the drivers of cardiac fibrillation in animal models and in humans. It is our prediction that in the next decade, more reliable and high-resolution methods and devices will be developed to identify rotors and spiral waves consistently during AF and VF in vivo. These studies will immensely benefit ablation and electric/defibrillator therapies in the short-term. However, we expect that as more mechanistic insights regarding the ionic/molecular basis of rotors continue to emerge, novel, more efficacious, and safer therapeutic approaches (either preventive or curative) will eventually come of age to provide relief from the debilitating and potentially lethal effects of rotors/fibrillation in less expensive ways to a much larger population worldwide.

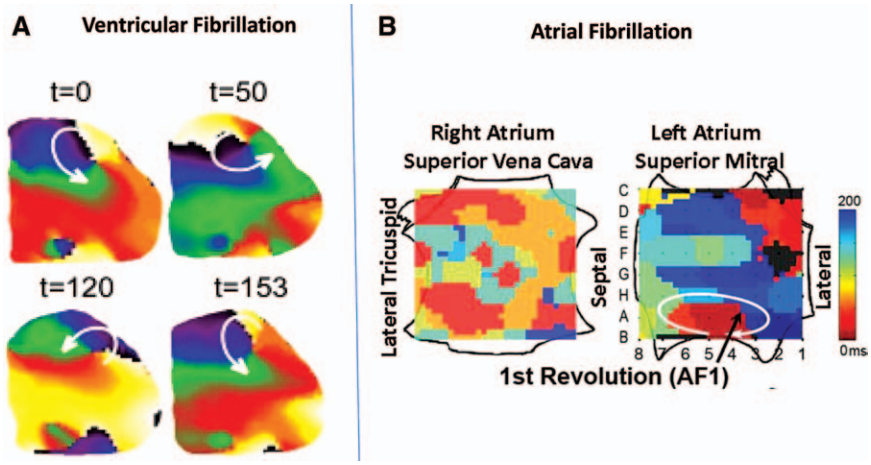

Figure 8. Rotors in human hearts. A, Sequential snapshots during a full rotation of a rotor located near the lateral wall of the left ventricle and generating ventricular fibrillation (VF) in a human heart mapped optically, in vitro (from Reference [72]). **B**, Left atrial rotor and fibrillatory conduction during atrial fibrillation (AF) in a human heart mapped electrically in vivo using 2 transvenous basket catheters simultaneously (modified from Reference [129] with permission of the authors and the publisher).

Acknowledgments

The authors thank Kate Campbell and Sergey Mironov for assistance with some of the figures.

Sources of Funding

Supported by National Heart, Lung, and Blood Institute grants P01HL039707 and P01HL087226 (to J. Jalife), Gilead, Inc (to J. Jalife and S.V. Pandit), and the Leducq Foundation (J. Jalife).

Disclosures

Dr Pandit received a research grant from Gilead, Inc. Dr Jalife received a research grant from Gilead, Inc, and is on the scientific advisory boards for Topera, Inc and Rhythm Solutions, Inc.

References

1. Jalife J. Déjà vu in the theories of atrial fibrillation dynamics. *Cardiovasc Res*. 2011;89:766–775.
2. Mayer J. *Rhythmical Pulsation in Scyphomedusae*. Washington, DC: Carnegie Institute of Washington; 1906:1–62. Publication number 47.
3. Mines GR. On dynamic equilibrium in the heart. *J Physiol (Lond)*. 1913;46:349–383.
4. Mines G. On circulating excitations in heart muscles and their possible relation to tachycardia and fibrillation. *Trans R Soc Can* 1914;4:43–52
5. Garrey W. The nature of fibrillary contraction of the heart: its relation to tissue mass and form. *Am J Physiol* 1914;33:397–414.
6. Lewis T. Oliver-Sharpey Lectures: On the nature of flutter and fibrillation of the auricle. *Br Med J*. 1921;1:590–593.
7. Lewis T. Oliver-Sharpey Lectures: On the nature of flutter and fibrillation of the auricle. *Br Med J*. 1921;1:551–555.
8. Lewis T. Observations upon flutter and fibrillation: II–The nature of auricular flutter. *Heart* 1920;7:191–233.
9. Wiener N, Rosenblueth A. The mathematical formulation of the problem of conduction of impulses in a network of connected excitable elements, specifically in cardiac muscle. *Arch Inst Cardiol Mex*. 1946;16:205–265.
10. Moe G. On the multiple wavelet hypothesis of atrial fibrillation. *Arch Int Pharmacodyn Ther* 1962;140:183–188.
11. Moe GK, Rheinboldt WC, Abildskov JA. A computer model of atrial fibrillation. *Am Heart J*. 1964;67:200–220.
12. Allessie MA, Bonke FI, Schopman FJ. Circus movement in rabbit atrial muscle as a mechanism of trachycardia. *Circ Res*. 1973;33:54–62.
13. Allessie MA, Bonke FI, Schopman FJ. Circus movement in rabbit atrial muscle as a mechanism of tachycardia: II--the role of nonuniform recovery of excitability in the occurrence of unidirectional block, as studied with multiple microelectrodes. *Circ Res*. 1976;39:168–177.
14. Allessie MA, Bonke FI, Schopman FJ. Circus movement in rabbit atrial muscle as a mechanism of tachycardia: III--the "leading circle" concept: a new model of circus movement in cardiac tissue without the involvement of an anatomical obstacle. *Circ Res*. 1977;41:9–18.
15. Allessie MA, Lammers WJEP, Bonke FIM, Hollen J. Experimental evaluation of Moe's multiple wavelet hypothesis of atrial fibrillation. In: Zipes DP, Jalife J, eds. *Cardiac electrophysiology and arrhythmias*. Orlando, FL: Grune & Stratton; 1985: 265–275.
16. Krinsky V. Spread of excitation in an inhomogeneous medium (state similar to cardiac fibrillation). *Biophysics*. 1966;11:676–683.
17. Winfree AT. *When time breaks down*. Princeton, NJ: Princeton University Press; 1987.
18. Davidenko JM, Kent PF, Chialvo DR, Michaels DC, Jalife J. Sustained vortex-like waves in normal isolated ventricular muscle. *Proc Natl Acad Sci USA*. 1990;87:8785–8789.
19. Salama G, Morad M. Merocyanine 540 as an optical probe of transmembrane electrical activity in the heart. *Science*. 1976;191:485–487.
20. Jalife J. Ventricular fibrillation: mechanisms of initiation and maintenance. *Annu Rev Physiol*. 2000;62:25–50.
21. Jalife J, Berenfeld O, Skanes A, Mandapati R. Mechanisms of atrial fibrillation: mother rotors or multiple daughter wavelets, or both? *J Cardiovasc Electrophysiol*. 1998;9:S2–12.
22. Witkowski FX, Leon LJ, Penkoske PA, Giles WR, Spano ML, Ditto WL, Winfree AT. Spatiotemporal evolution of ventricular fibrillation. *Nature*. 1998;392:78–82.
23. Eckstein J, Verheule S, de Groot NM, de Groot N, Allessie M, Schotten U. Mechanisms of perpetuation of atrial fibrillation in chronically dilated atria. *Prog Biophys Mol Biol*. 2008;97:435–451.
24. Tabereaux PB, Dosdall DJ, Ideker RE. Mechanisms of VF maintenance: wandering wavelets, mother rotors, or foci. *Heart Rhythm*. 2009;6:405–415.
25. Jalife J. Inward rectifier potassium channels control rotor frequency in ventricular fibrillation. *Heart Rhythm*. 2009;6:S44–S48.
26. Vaquero M, Calvo D, Jalife J. Cardiac fibrillation: from ion channels to rotors in the human heart. *Heart Rhythm*. 2008;5:872–879.
27. Berenfeld O, Pertsov AM. Dynamics of intramural scroll waves in three-dimensional continuous myocardium with rotational anisotropy. *J Theor Biol*. 1999;199:383–394.
28. Yamazaki M, Mironov S, Taravant C, Brec J, Vaquero LM, Bandaru K, Avula UM, Honjo H, Kodama I, Berenfeld O, Kalifa J. Heterogeneous atrial wall thickness and stretch promote scroll waves anchoring during atrial fibrillation. *Cardiovasc Res*. 2012;94:48–57.
29. Gray RA, Pertsov AM, Jalife J. Spatial and temporal organization during cardiac fibrillation. *Nature*. 1998;392:75–78.
30. Panfilov AV. Theory of reentry. In: Zipes DP, Jalife J, eds. *Cardiac electrophysiology: From cell to bedside*, 5th ed. Philadelphia, PA: Elsevier; 2009.
31. Fast VG, Kléber AG. Role of wavefront curvature in propagation of cardiac impulse. *Cardiovasc Res*. 1997;33:258–271.
32. Gray RA, Jalife J, Panfilov AV, Baxter WT, Cabo C, Davidenko JM, Pertsov AM. Mechanisms of cardiac fibrillation. *Science*. 1995;270:1222–1223; author reply 1224.
33. Blaauw Y, Gögelein H, Tieleman RG, van Hunnik A, Schotten U, Allessie MA. "Early" class III drugs for the treatment of atrial fibrillation: efficacy and atrial selectivity of AVE0118 in remodeled atria of the goat. *Circulation*. 2004;110:1717–1724.
34. Wijffels MC, Dorland R, Allessie MA. Pharmacologic cardioversion of chronic atrial fibrillation in the goat by class IA, IC, and III drugs: a comparison between hydroquinidine, cibenzoline, flecainide, and d-sotalol. *J Cardiovasc Electrophysiol*. 1999;10:178–193.
35. Wang J, Bourne GW, Wang Z, Villemaire C, Talajic M, Nattel S. Comparative mechanisms of antiarrhythmic drug action in experimental atrial fibrillation. Importance of use-dependent effects on refractoriness. *Circulation*. 1993;88:1030–1044.
36. Jalife J, Berenfeld O, Mansour M. Mother rotors and fibrillatory conduction: a mechanism of atrial fibrillation. *Cardiovasc Res*. 2002;54:204–216.
37. Wijffels MC, Dorland R, Mast F, Allessie MA. Widening of the excitable gap during pharmacological cardioversion of atrial fibrillation in the goat: effects of cibenzoline, hydroquinidine, flecainide, and d-sotalol. *Circulation*. 2000;102:260–267.
38. Pandit SV, Berenfeld O, Anumonwo JM, Zaritski RM, Kneller J, Nattel S, Jalife J. Ionic determinants of functional reentry in a 2-D model of human atrial cells during simulated chronic atrial fibrillation. *Biophys J*. 2005;88:3806–3821.
39. Courtemanche M, Ramirez RJ, Nattel S. Ionic mechanisms underlying human atrial action potential properties: insights from a mathematical model. *Am J Physiol*. 1998;275:H301–H321.
40. Courtemanche M, Ramirez RJ, Nattel S. Ionic targets for drug therapy and atrial fibrillation-induced electrical remodeling: insights from a mathematical model. *Cardiovasc Res*. 1999;42:477–489.
41. Luo CH, Rudy Y. A dynamic model of the cardiac ventricular action potential. I. Simulations of ionic currents and concentration changes. *Circ Res*. 1994;74:1071–1096.
42. Pandit SV, Warren M, Mironov S, Tolkacheva EG, Kalifa J, Berenfeld O, Jalife J. Mechanisms underlying the antifibrillatory action of hyperkalemia in Guinea pig hearts. *Biophys J*. 2010;98:2091–2101.
43. Weiss JN, Qu Z, Chen PS, Lin SF, Karagueuzian HS, Hayashi H, Garfinkel A, Karma A. The dynamics of cardiac fibrillation. *Circulation*. 2005;112:1232–1240.
44. Fox JJ, Riccio ML, Hua F, Bodenschatz E, Gilmour RF Jr. Spatiotemporal transition to conduction block in canine ventricle. *Circ Res*. 2002;90:289–296.
45. Cabo C, Pertsov AM, Davidenko JM, Jalife J. Electrical turbulence as a result of the critical curvature for propagation in cardiac tissue. *Chaos*. 1998;8:116–126.
46. Cabo C, Pertsov AM, Davidenko JM, Baxter WT, Gray RA, Jalife J. Vortex shedding as a precursor of turbulent electrical activity in cardiac muscle. *Biophys J*. 1996;70:1105–1111.
47. Luo CH, Rudy Y. A model of the ventricular cardiac action potential. Depolarization, repolarization, and their interaction. *Circ Res*. 1991;68:1501–1526.
48. Janse MJ, Wit AL. Electrophysiological mechanisms of ventricular arrhythmias resulting from myocardial ischemia and infarction. *Physiol Rev*. 1989;69:1049–1169.

49. Nattel S, Burstein B, Dobrev D. Atrial remodeling and atrial fibrillation: mechanisms and implications. *Circ Arrhythm Electrophysiol*. 2008;1:62–73.
50. Schotten U, Verheule S, Kirchhof P, Goette A. Pathophysiological mechanisms of atrial fibrillation: a translational appraisal. *Physiol Rev*. 2011;91:265–325.
51. Gray RA. Rotors and Spiral waves in the heart. In: Zipes DP, Jalife J, eds. *Cardiac electrophysiology: From cell to bedside*, 5th ed. Philadelphia, PA: Elsevier; 2009.
52. Bray MA, Wikswo JP. Considerations in phase plane analysis for nonstationary reentrant cardiac behavior. *Phys Rev E Stat Nonlin Soft Matter Phys*. 2002;65:051902.
53. Nash MP, Mourad A, Clayton RH, Sutton PM, Bradley CP, Hayward M, Paterson DJ, Taggart P. Evidence for multiple mechanisms in human ventricular fibrillation. *Circulation*. 2006;114:536–542.
54. Davidenko JM, Pertsov AV, Salomonsz R, Baxter W, Jalife J. Stationary and drifting spiral waves of excitation in isolated cardiac muscle. *Nature*. 1992;355:349–351.
55. Zlochiver S, Yamazaki M, Kalifa J, Berenfeld O. Rotor meandering contributes to irregularity in electrograms during atrial fibrillation. *Heart Rhythm*. 2008;5:846–854.
56. Skanes AC, Mandapati R, Berenfeld O, Davidenko JM, Jalife J. Spatiotemporal periodicity during atrial fibrillation in the isolated sheep heart. *Circulation*. 1998;98:1236–1248.
57. Chen J, Mandapati R, Berenfeld O, Skanes AC, Jalife J. High-frequency periodic sources underlie ventricular fibrillation in the isolated rabbit heart. *Circ Res*. 2000;86:86–93.
58. Asano Y, Davidenko JM, Baxter WT, Gray RA, Jalife J. Optical mapping of drug-induced polymorphic arrhythmias and torsade de pointes in the isolated rabbit heart. *J Am Coll Cardiol*. 1997;29:831–842.
59. Jalife J, Gray R. Drifting vortices of electrical waves underlie ventricular fibrillation in the rabbit heart. *Acta Physiol Scand*. 1996;157:123–131.
60. Berenfeld O, Mandapati R, Dixit S, Skanes AC, Chen J, Mansour M, Jalife J. Spatially distributed dominant excitation frequencies reveal hidden organization in atrial fibrillation in the Langendorff-perfused sheep heart. *J Cardiovasc Electrophysiol*. 2000;11:869–879.
61. Mansour M, Mandapati R, Berenfeld O, Chen J, Samie FH, Jalife J. Left-to-right gradient of atrial frequencies during acute atrial fibrillation in the isolated sheep heart. *Circulation*. 2001;103:2631–2636.
62. Pandit SV, Zlochiver S, Filgueiras-Rama D, Mironov S, Yamazaki M, Ennis SR, Noujaim SF, Workman AJ, Berenfeld O, Kalifa J, Jalife J. Targeting atrioventricular differences in ion channel properties for terminating acute atrial fibrillation in pigs. *Cardiovasc Res*. 2011;89:843–851.
63. Lazar S, Dixit S, Marchlinski FE, Callans DJ, Gerstenfeld EP. Presence of left-to-right atrial frequency gradient in paroxysmal but not persistent atrial fibrillation in humans. *Circulation*. 2004;110:3181–3186.
64. Sanders P, Berenfeld O, Hocini M, Jaïs P, Vaidyanathan R, Hsu LF, Garrigue S, Takahashi Y, Rotter M, Sacher F, Scavée C, Ploutz-Snyder R, Jalife J, Haïssaguerre M. Spectral analysis identifies sites of high-frequency activity maintaining atrial fibrillation in humans. *Circulation*. 2005;112:789–797.
65. Atienza F, Almendral J, Jalife J, Zlochiver S, Ploutz-Snyder R, Torrecilla EG, Arenal A, Kalifa J, Fernández-Avilés F, Berenfeld O. Real-time dominant frequency mapping and ablation of dominant frequency sites in atrial fibrillation with left-to-right frequency gradients predicts long-term maintenance of sinus rhythm. *Heart Rhythm*. 2009;6:33–40.
66. Samie FH, Berenfeld O, Anumonwo J, Mironov SF, Udassi S, Beaumont J, Taffet S, Pertsov AM, Jalife J. Rectification of the background potassium current: a determinant of rotor dynamics in ventricular fibrillation. *Circ Res*. 2001;89:1216–1223.
67. Sarmast F, Kolli A, Zaitsev A, Parisian K, Dhamoon AS, Guha PK, Warren M, Anumonwo JM, Taffet SM, Berenfeld O, Jalife J. Cholinergic atrial fibrillation: I(K,ACh) gradients determine unequal left/right atrial frequencies and rotor dynamics. *Cardiovasc Res*. 2003;59:863–873.
68. Jalife J. Rotors and spiral waves in atrial fibrillation. *J Cardiovasc Electrophysiol*. 2003;14:776–780.
69. Kalifa J, Tanaka K, Zaitsev AV, Warren M, Vaidyanathan R, Auerbach D, Pandit S, Vikstrom KL, Ploutz-Snyder R, Talkachou A, Atienza F, Guiraudon G, Jalife J, Berenfeld O. Mechanisms of wave fractionation at boundaries of high-frequency excitation in the posterior left atrium of the isolated sheep heart during atrial fibrillation. *Circulation*. 2006;113:626–633.
70. Campbell KF, Calvo CJ, Mironov S, Herron T, Berenfeld O, Jalife J. Spatial gradients in action potential duration created by regional magnetofection of hERG are a substrate for wavebreak and turbulent propagation in a rat cardiomyocyte monolayer model of cardiac fibrillation. *J Physiol*. 2012;590:6363–6379.
71. Zipes DP, Fischer J, King RM, Nicoll A deB, Jolly WW. Termination of ventricular fibrillation in dogs by depolarizing a critical amount of myocardium. *Am J Cardiol*. 1975;36:37–44.
72. Vaidya D, Morley GE, Samie FH, Jalife J. Reentry and fibrillation in the mouse heart. A challenge to the critical mass hypothesis. *Circ Res*. 1999;85:174–181.
73. Noujaim SF, Berenfeld O, Kalifa J, Cerrone M, Nanthakumar K, Atienza F, Moreno J, Mironov S, Jalife J. Universal scaling law of electrical turbulence in the mammalian heart. *Proc Natl Acad Sci USA*. 2007;104:20985–20989.
74. Noujaim SF, Lucca E, Muñoz V, Persaud D, Berenfeld O, Meijler FL, Jalife J. From mouse to whale: a universal scaling relation for the PR Interval of the electrocardiogram of mammals. *Circulation*. 2004;110:2802–2808.
75. Haïssaguerre M, Jaïs P, Shah DC, Takahashi A, Hocini M, Quiniou G, Garrigue S, Le Mouroux A, Le Métayer P, Clémenty J. Spontaneous initiation of atrial fibrillation by ectopic beats originating in the pulmonary veins. *N Engl J Med*. 1998;339:659–666.
76. Ho SY, Cabrera JA, Sanchez-Quintana D. Left atrial anatomy revisited. *Circ Arrhythm Electrophysiol*. 2012;5:220–228.
77. Klos M, Calvo D, Yamazaki M, Zlochiver S, Mironov S, Cabrera JA, Sanchez-Quintana D, Jalife J, Berenfeld O, Kalifa J. Atrial septopulmonary bundle of the posterior left atrium provides a substrate for atrial fibrillation initiation in a model of vagally mediated pulmonary vein tachycardia of the structurally normal heart. *Circ Arrhythm Electrophysiol*. 2008;1:175–183.
78. Moe GK, Mendez C. Functional block in the intraventricular conduction system. *Circulation*. 1971;43:949–954.
79. Fast VG, Kléber AG. Cardiac tissue geometry as a determinant of unidirectional conduction block: assessment of microscopic excitation spread by optical mapping in patterned cell cultures and in a computer model. *Cardiovasc Res*. 1995;29:697–707.
80. Filgueiras-Rama D, Price NF, Martins RP, Yamazaki M, Avula UM, Kaur K, Kalifa J, Ennis SR, Hwang E, Devabhaktuni V, Jalife J, Berenfeld O. Long-term frequency gradients during persistent atrial fibrillation in sheep are associated with stable sources in the left atrium. *Circ Arrhythm Electrophysiol*. 2012;5:1160–1167.
81. Kim YH, Xie F, Yashima M, Wu TJ, Valderrábano M, Lee MH, Ohara T, Voroshilovsky O, Doshi RN, Fishbein MC, Qu Z, Garfinkel A, Weiss JN, Karagueuzian HS, Chen PS. Role of papillary muscle in the generation and maintenance of reentry during ventricular tachycardia and fibrillation in isolated swine right ventricle. *Circulation*. 1999;100:1450–1459.
82. Auerbach DS, Grzda KR, Furspan PB, Sato PY, Mironov S, Jalife J. Structural heterogeneity promotes triggered activity, reflection and arrhythmogenesis in cardiomyocyte monolayers. *J Physiol (Lond)*. 2011;589:2363–2381.
83. Bian W, Tung L. Structure-related initiation of reentry by rapid pacing in monolayers of cardiac cells. *Circ Res*. 2006;98:e29–e38.
84. Warren M, Guha PK, Berenfeld O, Zaitsev A, Anumonwo JM, Dhamoon AS, Bagwe S, Taffet SM, Jalife J. Blockade of the inward rectifying potassium current terminates ventricular fibrillation in the guinea pig heart. *J Cardiovasc Electrophysiol*. 2003;14:621–631.
85. Samie FH, Mandapati R, Gray RA, Watanabe Y, Zuur C, Beaumont J, Jalife J. A mechanism of transition from ventricular fibrillation to tachycardia: effect of calcium channel blockade on the dynamics of rotating waves. *Circ Res*. 2000;86:684–691.
86. Kneller J, Kalifa J, Zou R, Zaitsev AV, Warren M, Berenfeld O, Vigmond EJ, Leon LJ, Nattel S, Jalife J. Mechanisms of atrial fibrillation termination by pure sodium channel blockade in an ionically-realistic mathematical model. *Circ Res*. 2005;96:e35–e47.
87. Comtois P, Sakabe M, Vigmond EJ, Munoz M, Texier A, Shiroshita-Takeshita A, Nattel S. Mechanisms of atrial fibrillation termination by rapidly unbinding Na+ channel blockers: insights from mathematical models and experimental correlates. *Am J Physiol Heart Circ Physiol*. 2008;295:H1489–H1504.
88. Qu Z, Weiss JN. Effects of Na(+) and K(+) channel blockade on vulnerability to and termination of fibrillation in simulated normal cardiac tissue. *Am J Physiol Heart Circ Physiol*. 2005;289:H1692–H1701.
89. Starmer CF, Romashko DN, Reddy RS, Zilberter YI, Starobin J, Grant AO, Krinsky VI. Proarrhythmic response to potassium channel blockade. Numerical studies of polymorphic tachyarrhythmias. *Circulation*. 1995;92:595–605.

90. Blaauw Y, Schotten U, van Hunnik A, Neuberger HR, Allessie MA. Cardioversion of persistent atrial fibrillation by a combination of atrial specific and non-specific class III drugs in the goat. *Cardiovasc Res*. 2007;75:89–98.
91. Wijffels MC, Dorland R, Allessie MA. Pharmacologic cardioversion of chronic atrial fibrillation in the goat by class IA, IC, and III drugs: a comparison between hydroquinidine, cibenzoline, flecainide, and d-sotalol. *J Cardiovasc Electrophysiol*. 1999;10:178–193.
92. Ishiguro YS, Honjo H, Opthof T, Okuno Y, Nakagawa H, Yamazaki M, Harada M, Takanari H, Suzuki T, Morishima M, Sakuma I, Kamiya K, Kodama I. Early termination of spiral wave reentry by combined blockade of Na+ and L-type Ca2+ currents in a perfused two-dimensional epicardial layer of rabbit ventricular myocardium. *Heart Rhythm*. 2009;6:684–692.
93. Yamazaki M, Honjo H, Nakagawa H, Ishiguro YS, Okuno Y, Amino M, Sakuma I, Kamiya K, Kodama I. Mechanisms of destabilization and early termination of spiral wave reentry in the ventricle by a class III antiarrhythmic agent, nifekalant. *Am J Physiol Heart Circ Physiol*. 2007;292:H539–H548.
94. Choi BR, Liu T, Salama G. The distribution of refractory periods influences the dynamics of ventricular fibrillation. *Circ Res*. 2001;88:E49–E58.
95. Nerbonne JM, Nichols CG, Schwarz TL, Escande D. Genetic manipulation of cardiac K(+) channel function in mice: what have we learned, and where do we go from here? *Circ Res*. 2001;89:944–956.
96. Rohr S, Schölly DM, Kléber AG. Patterned growth of neonatal rat heart cells in culture. Morphological and electrophysiological characterization. *Circ Res*. 1991;68:114–130.
97. Bursac N, Aguel F, Tung L. Multiarm spirals in a two-dimensional cardiac substrate. *Proc Natl Acad Sci USA*. 2004;101:15530–15534.
98. Pandit SV, Clark RB, Giles WR, Demir SS. A mathematical model of action potential heterogeneity in adult rat left ventricular myocytes. *Biophys J*. 2001;81:3029–3051.
99. Bondarenko VE, Szigeti GP, Bett GC, Kim SJ, Rasmusson RL. Computer model of action potential of mouse ventricular myocytes. *Am J Physiol Heart Circ Physiol*. 2004;287:H1378–H1403.
100. Beaumont J, Davidenko N, Davidenko JM, Jalife J. Spiral waves in two-dimensional models of ventricular muscle: formation of a stationary core. *Biophys J*. 1998;75:1–14.
101. Van Wagoner DR, Pond AL, McCarthy PM, Trimmer JS, Nerbonne JM. Outward K+ current densities and Kv1.5 expression are reduced in chronic human atrial fibrillation. *Circ Res*. 1997;80:772–781.
102. Dobrev D, Wettwer E, Himmel HM, Kortner A, Kuhlisch E, Schüler S, Siffert W, Ravens U. G-Protein beta(3)-subunit 825T allele is associated with enhanced human atrial inward rectifier potassium currents. *Circulation*. 2000;102:692–697.
103. Voigt N, Trausch A, Knaut M, Matschke K, Varró A, Van Wagoner DR, Nattel S, Ravens U, Dobrev D. Left-to-right atrial inward rectifier potassium current gradients in patients with paroxysmal versus chronic atrial fibrillation. *Circ Arrhythm Electrophysiol*. 2010;3:472–480.
104. Li J, McLerie M, Lopatin AN. Transgenic upregulation of IK1 in the mouse heart leads to multiple abnormalities of cardiac excitability. *Am J Physiol Heart Circ Physiol*. 2004;287:H2790–H2802.
105. Noujaim SF, Pandit SV, Berenfeld O, Vikstrom K, Cerrone M, Mironov S, Zugermayr M, Lopatin AN, Jalife J. Up-regulation of the inward rectifier K+ current (I K1) in the mouse heart accelerates and stabilizes rotors. *J Physiol (Lond)*. 2007;578:315–326.
106. Nerbonne JM, Kass RS. Molecular physiology of cardiac repolarization. *Physiol Rev*. 2005;85:1205–1253.
107. Muñoz V, Grzeda KR, Desplantez T, Pandit SV, Mironov S, Taffet SM, Rohr S, Kléber AG, Jalife J. Adenoviral expression of IKs contributes to wavebreak and fibrillatory conduction in neonatal rat ventricular cardiomyocyte monolayers. *Circ Res*. 2007;101:475–483.
108. Hou L, Deo M, Furspan P, Pandit SV, Mironov S, Auerbach DS, Gong Q, Zhou Z, Berenfeld O, Jalife J. A major role for HERG in determining frequency of reentry in neonatal rat ventricular myocyte monolayer. *Circ Res*. 2010;107:1503–1511.
109. Delmar M, Glass L, Michaels DC, Jalife J. Ionic basis and analytical solution of the wenckebach phenomenon in guinea pig ventricular myocytes. *Circ Res*. 1989;65:775–788.
110. Delmar M, Michaels DC, Jalife J. Slow recovery of excitability and the Wenckebach phenomenon in the single guinea pig ventricular myocyte. *Circ Res*. 1989;65:761–774.
111. Sekar RB, Kizana E, Cho HC, Molitoris JM, Hesketh GG, Eaton BP, Marbán E, Tung L. IK1 heterogeneity affects genesis and stability of spiral waves in cardiac myocyte monolayers. *Circ Res*. 2009;104:355–364.
112. Bers DM. *Excitation-contraction coupling and cardiac contractile force*. Dordrecht, the Netherlands: Kluwer Academic Publishers; 2001.
113. Zhang S, Zhou Z, Gong Q, Makielski JC, January CT. Mechanism of block and identification of the verapamil binding domain to HERG potassium channels. *Circ Res*. 1999;84:989–998.
114. Warren M, Zaitsev AV. Evidence against the role of intracellular calcium dynamics in ventricular fibrillation. *Circ Res*. 2008;102:e103.
115. Warren M, Huizar JF, Shvedko AG, Zaitsev AV. Spatiotemporal relationship between intracellular Ca2+ dynamics and wave fragmentation during ventricular fibrillation in isolated blood-perfused pig hearts. *Circ Res*. 2007;101:e90–e101.
116. Ogawa M, Lin SF, Weiss JN, Chen PS. Calcium dynamics and ventricular fibrillation. *Circ Res*. 2008;102:e52.
117. Choi BR, Burton F, Salama G. Cytosolic Ca2+ triggers early afterdepolarizations and Torsade de Pointes in rabbit hearts with type 2 long QT syndrome. *J Physiol (Lond)*. 2002;543:615–631.
118. Cerrone M, Noujaim SF, Tolkacheva EG, Talkachou A, O'Connell R, Berenfeld O, Anumonwo J, Pandit SV, Vikstrom K, Napolitano C, Priori SG, Jalife J. Arrhythmogenic mechanisms in a mouse model of catecholaminergic polymorphic ventricular tachycardia. *Circ Res*. 2007;101:1039–1048.
119. Mandapati R, Asano Y, Baxter WT, Gray R, Davidenko J, Jalife J. Quantification of effects of global ischemia on dynamics of ventricular fibrillation in isolated rabbit heart. *Circulation*. 1998;98:1688–1696.
120. Papadatos GA, Wallerstein PM, Head CE, Ratcliff R, Brady PA, Benndorf K, Saumarez RC, Trezise AE, Huang CL, Vandenberg JI, Colledge WH, Grace AA. Slowed conduction and ventricular tachycardia after targeted disruption of the cardiac sodium channel gene Scn5a. *Proc Natl Acad Sci USA*. 2002;99:6210–6215.
121. Noujaim SF, Stuckey JA, Ponce-Balbuena D, Ferrer-Villada T, López-Izquierdo A, Pandit SV, Sánchez-Chapula JA, Jalife J. Structural bases for the different anti-fibrillatory effects of chloroquine and quinidine. *Cardiovasc Res*. 2011;89:862–869.
122. Filgueiras-Rama D, Martins RP, Mironov S, Yamazaki M, Calvo CJ, Ennis SR, Bandaru K, Noujaim SF, Kalifa J, Berenfeld O, Jalife J. Chloroquine terminates stretch-induced atrial fibrillation more effectively than flecainide in the sheep heart. *Circ Arrhythm Electrophysiol*. 2012;5:561–570.
123. Yamazaki M, Honjo H, Ashihara T, Harada M, Sakuma I, Nakazawa K, Trayanova N, Horie M, Kalifa J, Jalife J, Kamiya K, Kodama I. Regional cooling facilitates termination of spiral-wave reentry through unpinning of rotors in rabbit hearts. *Heart Rhythm*. 2012;9:107–114.
124. Krogh-Madsen T, Abbott GW, Christini DJ. Effects of electrical and structural remodeling on atrial fibrillation maintenance: a simulation study. *PLoS Comput Biol*. 2012;8:e1002390.
125. Bernus O, Van Eyck B, Verschelde H, Panfilov AV. Transition from ventricular fibrillation to ventricular tachycardia: a simulation study on the role of Ca(2+)-channel blockers in human ventricular tissue. *Phys Med Biol*. 2002;47:4167–4179.
126. ten Tusscher KH, Mourad A, Nash MP, Clayton RH, Bradley CP, Paterson DJ, Hren R, Hayward M, Panfilov AV, Taggart P. Organization of ventricular fibrillation in the human heart: experiments and models. *Exp Physiol*. 2009;94:553–562.
127. Massé S, Downar E, Chauhan V, Sevaptsidis E, Nanthakumar K. Ventricular fibrillation in myopathic human hearts: mechanistic insights from in vivo global endocardial and epicardial mapping. *Am J Physiol Heart Circ Physiol*. 2007;292:H2589–H2597.
128. Nair K, Umapathy K, Farid T, Masse S, Mueller E, Sivanandan RV, Poku K, Rao V, Nair V, Butany J, Ideker RE, Nanthakumar K. Intramural activation during early human ventricular fibrillation. *Circ Arrhythm Electrophysiol*. 2011;4:692–703.
129. Narayan SM, Krummen DE, Rappel WJ. Clinical mapping approach to diagnose electrical rotors and focal impulse sources for human atrial fibrillation. *J Cardiovasc Electrophysiol*. 2012;23:447–454.
130. Narayan SM, Krummen DE, Shivkumar K, Clopton P, Rappel WJ, Miller JM. Treatment of atrial fibrillation by the ablation of localized sources: CONFIRM (Conventional Ablation for Atrial Fibrillation With or Without Focal Impulse and Rotor Modulation) trial. *J Am Coll Cardiol*. 2012;60:628–636.